

Project Title: Small Unmanned Aircraft thermal infrared imaging system to identify soybean drought tolerant varieties

Final Report: 2017 - 2018

Authors: Ajay Sharda, William Schapaugh, Deon van der Merwe, Daniel Flippo,

Study Area

The study area is located at the Kansas State University, Kansas River Valley Experiment Field outside Rossville, KS (39.11852°, -95.92459°) and was selected for its prevalent SDS history. The dominant soil in the field is Eudora silt loam. Irrigation was applied throughout the growing season to maintain adequate soil moisture and to help increase the severity of SDS.

All plots had maturity and SDS ratings collected. Maturity was recorded as the number of days following 31 August when 95% of the pods on the plants had reached mature color. SDS ratings were taken at the R6 growth stage of the plants (Fehr et al., 1971).

The experiment consisted of a Nested Association Mapping (NAM) population comprised of 140 F₅ derived lines from a cross between IA3023 and LD00-3309 along with checks for yield, and agronomic traits and susceptible and resistant checks for resistance to Soybean Sudden Death Syndrome (SDS), for 160 entries. Four replications occurred for entries in the NAM population. The NAM population used a randomized complete block design using two-row plots 3.8 m long with 0.76 m between rows, and henceforth will be mentioned as plots for aerial imagery analysis. The field was planted on 9 May 2017 into corn stubble and application of pre-emergence herbicide prevented early season weed growth. Postemergence herbicide applications and hand weeding controlled weeds throughout the season.

SDS Scoring

SDS was scored on two criteria, severity and incidence. Severity (Ds) addresses the severity of the SDS infection based foliar symptoms, on a scale of 0-9, as seen in Table 1. Incidence (Di) accounts for the percentage of the plot infected with SDS. Incidence ranges from 0% to 100% in 5% increments. Scoring occurred at growth stage R6. R6 is the growth stage where the seedpod cavity is filled, and seeds are just reaching full size. R6 is designated for SDS scoring due to the expression of the disease symptoms (Schmidt, 2007).

Table 1 - SDS severity scoring guidelines

<i>Score</i>	<i>Description of Symptoms</i>
0	No visual evidence of infection
1	1-10% of leaf surface chlorotic, OR 1-5% necrotic
2	10-20% of leaf surface chlorotic, OR 6-10% necrotic
3	20-40% of leaf surface chlorotic, OR 11-20% necrotic
4	40-60% of leaf surface chlorotic, OR 21-40% necrotic
5	Greater than 60% of leaf surface chlorotic, OR greater than 40% necrotic
6	Premature leaf drop up to 1/3 defoliation
7	Premature leaf drop up to 2/3 defoliation
8	Premature leaf drop GREATER than 2/3 defoliation
9	Premature death

Once severity and incidence for the plot have been assessed they are used to establish the SDS score (Dx) using Equation 1 (Nijti et al., 2001). Dx ranges from 0-100. Scoring occurred on 6

September 2017 for the plots in this study. The same individual, to reduce error, completed scoring. Dx scores above 25 indicate severe SDS infection.

$$D_x = \frac{D_i * D_s}{9} \quad \text{Equation 1}$$

Where

Dx = SDS Score

Di = Incidence of infection

Ds = Severity of infection

Thermal Imagery

Aerial imagery was acquired using a sUAS coupled with a thermal camera designed for sUAS use. The IRIS+ (3DR, Berkeley, California, USA) in combination with a FLIR VUE Pro R 19 mm thermal camera (FLIR Systems, Wilsonville, Oregon, USA) captured imagery for this study. The thermal camera measures a spectral band from 7.5-13.5 μm .

Flight Planning

Flights occurred four times throughout the season on 28 August, 3 September, 8 September, and 13 September. Flights began at 12:00 p.m. on each day. A flight altitude 77 m above ground level (AGL) allowed a flight time of 7 minutes covering an area of about 1.8 hectares with a spatial resolution of 6.89 cm/pixel. Side lap was set to 75% while front-to-back overlap was set to 85% to achieve a one-second camera trigger interval. The sUAS was programmed to fly at a ground speed of 3 m/s. Based on the preliminary studies conducted with different ground speeds, the 3 m/s ground speed provided images with minimal blur.

Reference panels were instrumented to measure actual temperature and use it to calibrate canopy temperatures derived from images. Temperatures of reference panels were measured using surface-mounted thermistors (ON-930-44033, Omega Engineering Inc., Stamford, Connecticut, USA) with a measurement accuracy of $\pm 0.1^\circ\text{C}$. Reference panels were painted black, grey, white and another as water bath. The different colored panels and water bath provided different temperature gradients for canopy temperature calibration. Laboratory experiments showed that reference panels have uniform temperature across the surface. Air temperature and humidity were gathered using a humidity/temperature transmitter (HX303AV, Omega Engineering Inc., Stamford, Connecticut, USA) with an accuracy of $\pm 3\%$ and $\pm 0.2^\circ\text{C}$, respectively. Weather conditions for all flights were clear and atmospherically stable with minimal wind.

Data processing

Sixteen plots each with high (SDS score of 25 and over), medium (SDS score of 8-17), and low (SDS score of 0-5) SDS were randomly selected for comparison for a total of 48 plots. Independent images from each day were analyzed in FLIR Tools (FLIR Systems, Wilsonville, Oregon, USA) to derive the canopy temperature of each plot. Temperature was derived from the emitted radiation of the plot captured by the sensor. FLIR Tools used the target's emissivity, distance from the sensor to object (flight altitude AGL), relative humidity, and atmospheric temperature to derive the temperature. Emissivity was set at 0.94 nm (Guoquan & Zhengzhi, 1993; Rubio et al., 1997). Distance, relative humidity, and atmospheric temperature were set in camera settings in the field each day based on the daily conditions. Derived plot temperature was taken as the average temperature for that plot on a given day. The plots had complete canopy closure with no soil visible in the background; therefore area of each plot was drawn to derive average plot canopy temperature. The derived canopy temperature for each plot was averaged over five images. The images selected were five consecutive images with target plot visible in the middle during a single pass of the flight. Averaging over seven images eliminated bias that could occur due to changes in the angle between the canopy and sensor.

The canopy temperature (T_c) was extracted for each plot for each day as the average canopy temperature over five subsequent images and one left and right.

Derived temperatures were calibrated with infield calibration panels to account for error in the derivation of temperature from emitted radiance. Measured panel temperatures and temperatures of panels derived from FLIR Tools were used to create a regression line for calibration of canopy temperatures.

Average air temperature during flight was used to normalize the canopy temperature due to the large range in daily temperatures occurring over the study period, similar to work by Berni et al. (2009), Calderón et al. (2013), and Calderón et al. (2014a). The temperature difference was found using Equation 2 given below:

$$T_{\Delta} = T_c - T_a \quad \text{Equation 2}$$

Where

T_{Δ} = temperature difference

T_c = average canopy temperature

T_a = average air temperature during the flight

R statistical software was used to complete ANOVA testing and generate Spearman's rho correlations for each day.

Results

SDS Quantification

Average canopy temperature for all four flying dates varied between 66.1° F and 86.7° F, with standard deviation varying from 0.32° F to 7.65° F. Six plots (two low, two medium, and two high scoring) were chosen in the example. These results indicated the TIR sensor had a very consistent response to canopy emittance for series of images taken over the plots. It is also evident from the results that the canopy temperature was consistent when capturing canopy emitted radiation from different angles during multiple passes of the flight. Overall, these observations exhibited that averaging of TIR image data may not necessarily give improved results during spatial analysis of aerial imagery.

Temperature difference was compared to SDS scoring for each day flown to assess the relationship between temperature and SDS prevalence for each day. Each study period presented significance ($P < 0.0001$) in the relationship between temperature and SDS score, incidence, and severity. Figure 1 displays the temperature difference of each day compared to SDS score. Analysis of each flight revealed a progression in correlation between temperature difference and SDS scores. Spearman's rho correlation increases throughout the growing season with a moderate correlation observed for 28 August ($\rho = 0.5332$) and the strongest correlation observed for 13 September ($\rho = 0.7404$). Temperature difference exhibited a positive correlation to the SDS score for each day, which implies that a higher temperature difference represents a higher SDS score. 8 September exhibited noticeably high temperature difference values indicating canopy temperatures were above the air temperature. The temperature difference drops to much lower values on 13 September indicating low canopy temperatures relative to air temperature.

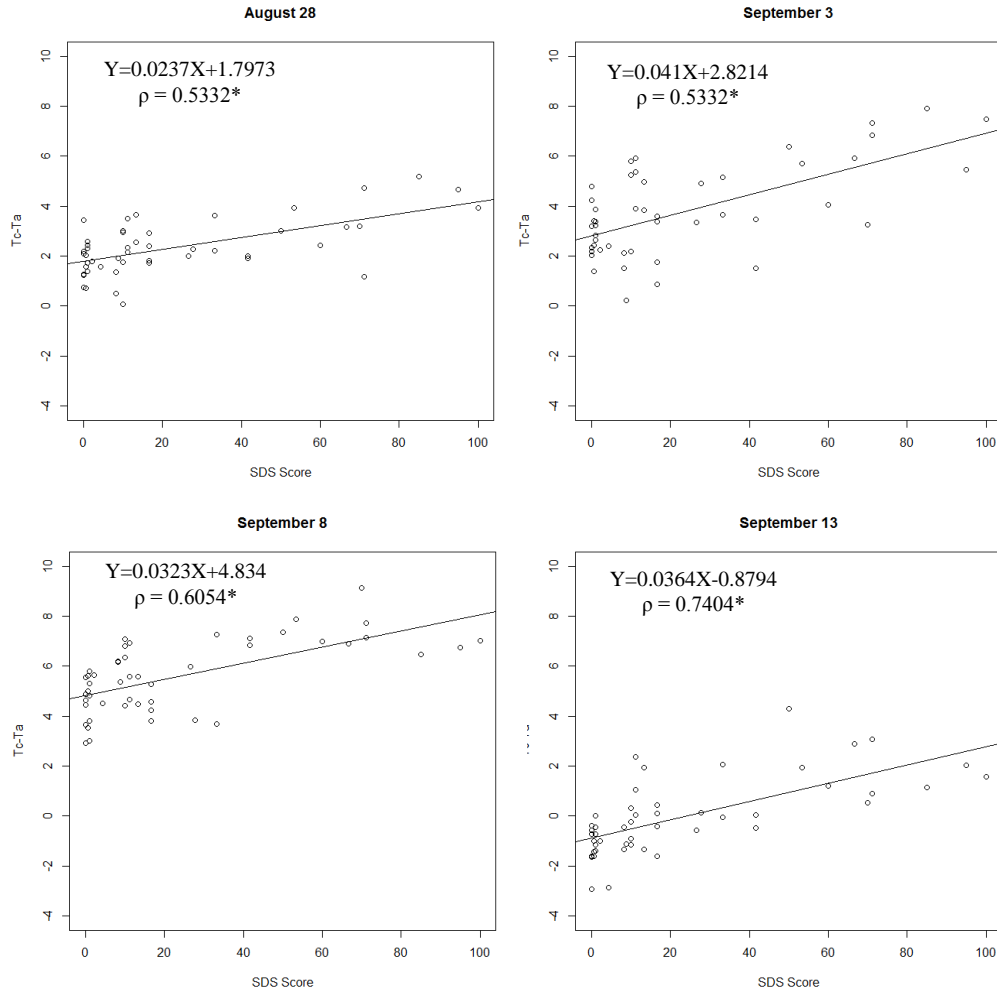


Figure 1 - SDS score to Tc-Ta (temperature difference) for each day of UAS flight. Equation for line of fit and Spearman's rho (ρ) are given for each plot. Correlation coefficients that were statistically significant ($P<0.0001$) are indicated by an asterisk.

Strong correlation was observed between temperature difference and SDS severity and incidence for each of the four sUAS flights. Figure 2 and Figure 3 show the severity and incidence, respectively, for each day of sUAS flight as compared to Tc-Ta (temperature difference). Both severity and incidence displayed similar statistical significance and correlation to the SDS score for a given day. As evident in Figure 1, both severity and incidence for 8 September displayed a much higher Tc-Ta (temperature difference) value and low temperature difference on 13 September compared to other days of flight. The high temperature difference could be due to unseasonably cool nightly temperatures. This value also exhibits a positive correlation to temperature difference. The general trend for each day demonstrates that higher temperature reflected greater extent of SDS infection in plant within a plot. The overall increase in correlation demonstrates the progression of the disease over the growing season. Symptoms reach maximum expression by the end of the season. However, affected plots begin presenting significant symptoms two weeks earlier than typically measured with current assessment methods (i.e. SDS scoring). 28 August exhibited few visual symptoms of SDS but exhibited higher temperatures due to stress caused by SDS. Early detection of SDS infection could lead to increased yields as mitigation steps could be implemented before visual symptoms develop.

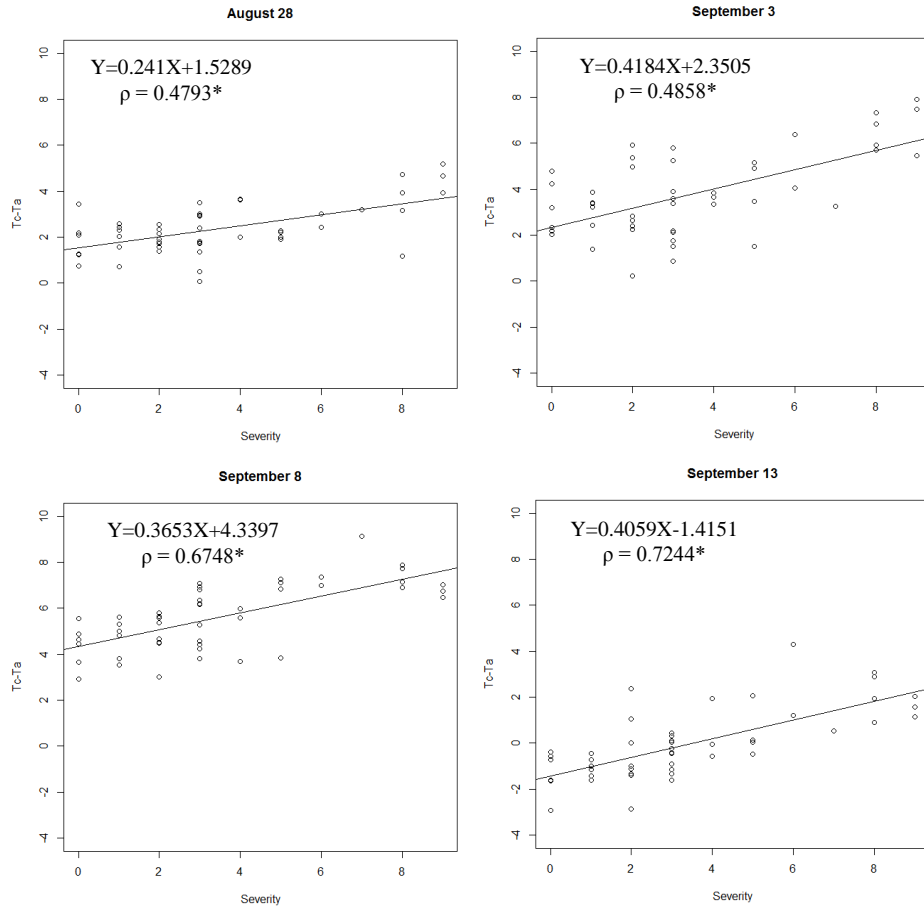


Figure 2 - Severity of infection to Tc-Ta (temperature difference for each day of UAS flight. Equation for line of fit and Spearman's rho (ρ) are given for each plot. Correlation coefficients that were statistically significant ($P < 0.0001$) are indicated by an asterisk.

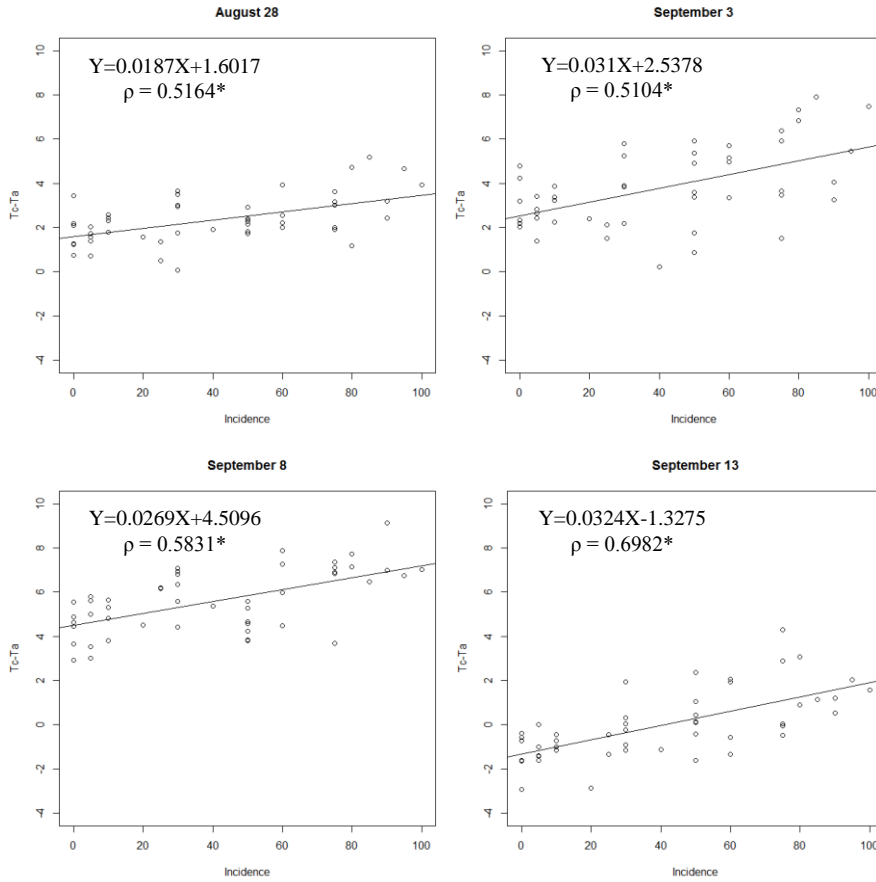


Figure 3 - Incidence of infection to Tc-Ta (temperature difference) for each day of UAS flight. Equation for line of fit and Spearman's rho (ρ) are given for each plot. Correlation coefficients that statistically significant ($P < 0.0001$) are indicated by an asterisk.

Spearman's rho plotted for SDS score, severity, and incidence displayed with R^2 values of 0.808, 0.8024, and 0.8622, respectively (Figure 4). Incidence shows the strongest relationship with R^2 at 0.8622. These graphs demonstrated how increasing temperatures led to increasing correlations as symptoms progressed. Symptom progression allowed for differentiation between temperatures of healthy and diseased plants. Early in symptom development temperatures of healthy plants and diseased plants showed moderate differentiation, however, as the disease progresses and symptom expression becomes greater the differentiation in temperature becomes stronger.

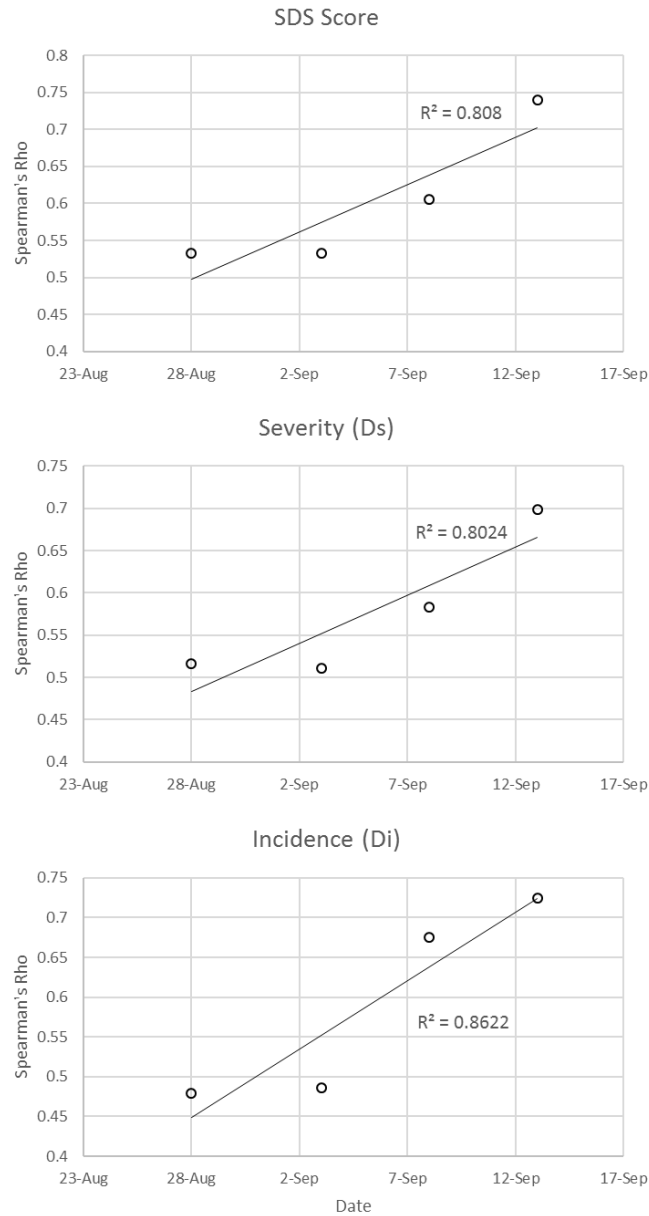


Figure 4 - Spearman's Rho related to SDS score, severity of infection, and incidence of infection. R² given for SDS score, severity, and incidence.

Discussion

Visual SDS symptoms on 28 August were minimal. A few plots exhibited chlorotic spots, but none exhibited necrotic spots. This day moderate correlations between temperature difference and SDS score, severity, and incidence. All correlations on 28 Aug were statistically significant. At this point in plant and disease development, the early stages of symptoms are not advanced enough to show strong correlations due to the limited symptom expression. SDS infection at this point in the season will be minimal only affecting a few plants. Plants showing marginal symptoms might not exhibit distinctly different temperature compared to healthy plants (Figure 5). Plots with low SDS infection are distinguished by a low temperature difference. Highly infected plots maintain high Tc-Ta values (Figure 5) across the four sUAS flight days. By 13 September, plots with high SDS scores

exhibited extreme symptoms with several plots dropping pods and exhibiting prematurely dead leaves. Strong, significant Spearman's rho correlations with temperature difference and SDS score, incidence, and severity ($P < 0.0001$) appear at this time.

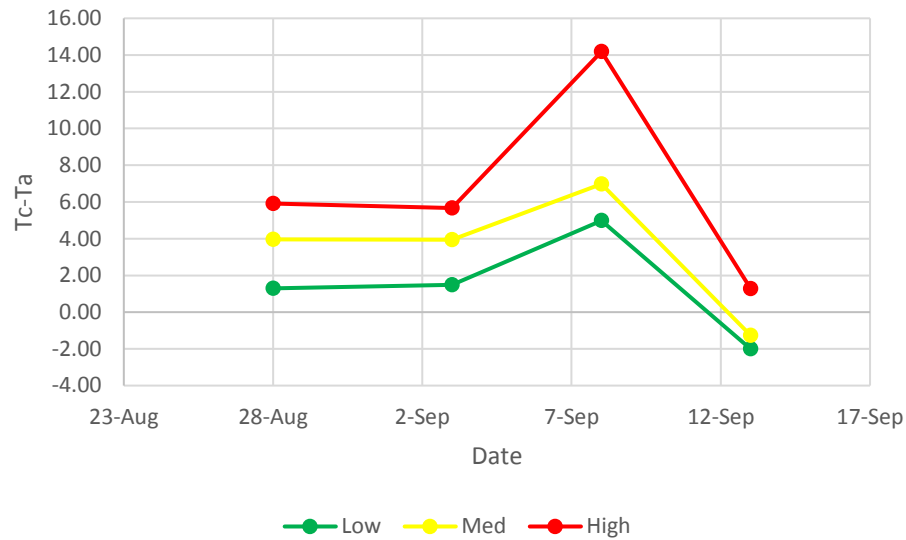


Figure 5 - Low, medium, and high plot across four sUAS flight days

An understanding of how field elements and weather affects a crop is critical to precision agriculture. Reasons explaining the observed correlation differences and changes in temperatures would be difficult without a thorough understanding of daily weather measurements. Large scale application of thermal remote sensing should include daily weather measurements and field factors to assess the sensed image accurately. 28 August and 3 September maintain temperature difference values ranging from 8 to -1. 8 September temperature difference values range from 10 to 2. 13 September temperature difference ranges from 5 to -3. The high-temperature difference values could be a result of increased canopy temperatures across the entire field.

Several uncharacteristically cool evenings between 4 September and 8 September explain the increase in temperature difference on 8 September. Evenings during this time dropped below 50⁰ F (10⁰ C). Temperatures this cool, are uncharacteristic for this region and time of year. Cool temperatures help SDS progress and can make symptoms worse. However, at this growth stage, the cool temperature could affect the plant health more than the development and progression of SDS. These cool evening temperatures can cause the plant to slow its metabolic processes. Photosynthesis, homeostasis, and transportation can all slow when cool weather is present. During this time, daily temperatures reached above 80⁰ F (27⁰ C). The combination of slowed transpiration and hot daily temperatures causes the plant have elevated canopy temperatures regardless of SDS infection. This can cause the canopy temperatures to rise across the whole field similar to what is seen on 8 September. All plots on 8 September exhibited higher temperatures including the plots unaffected by SDS. Increased canopy temperatures make it more difficult to distinguish between SDS and other factors affecting the plants such as non-disease stress. The overall range of temperatures increased for 8 September indicated by increased temperature difference to SDS score correlation. 13 September did not increase temperature difference rather temperature difference decreased. 13 September did not see the same effects on temperature difference as night temperatures after 8 September rose, and the soybeans recovered to resume normal metabolic processes.

Realistically, farmers with large fields cannot assess their entire crop for SDS on a daily or even weekly basis. Farmers would be unable to visually detect SDS in remote areas of the field until symptoms become severe.

Soybeans within a normal grow operation will not be scored for the incidence in a similar manner as they are for research plots. For remote sensing applications presented here to be effective on a large scale, it is critical that the severity and SDS score display similar correlations to temperature difference. Assessment of severity independently, seen in Figure 2 and Figure 4, express that severity very closely follows the correlation to temperature that SDS score displays. Plots of the Spearman's rho over the four days indicate similar relationship ($R^2=0.8024$) to Spearman's rho for SDS score. This strong relationship indicates that severity is a very good predictor of Spearman's rho for the given day. Farming applications can use TIR imagery for scouting a field for plots exhibiting high canopy temperatures as an indicator of SDS presence within their field.

Drought Stress Quantification

All the plots with drought studies setup in Salina were severely affected by Dicamba drift. A few plots which were Dicamba resistant were compared with non-resistant to Dicamba were compared. The results showed a significant difference in the canopy temperatures between the two varieties (Table 2). Several plots studies have been setup in Topeka, Rossville, Wamego and Ashland bottom to collect aerial imagery for drought resistant varieties in 2018. Aerial imagery on the study plots will be conducted from July through September, 2018.

Table 2 – Average Canopy Temperature of Dicamba resistant and non-resistant varieties.

Row	PI	Temperature
Column 4-9, S46XS87, Dicamba resistant		
1	0.004	44.4
2	0.034	44.8
3	0.025	45.3
4	0.025	45.5
Column 7-2, MG3.5, Dicamba non-resistant		
1	-0.097	50.9
2	-0.113	48.8
3	-0.114	48.7
4	-0.101	48.3

CIR Imagery Methods

Ground-based Plant Health

Ground-based measurements were collected from near canopy closure to R7 growth stage and the start of maturity (Fehr & Caviness, 1977). Data was collected on cloud-free days between 10 a.m. and 2 p.m. to limit solar effects. Two Ocean Optics USB2000 hyperspectral spectrometers (Ocean Optics, Largo, Florida, USA) were mounted on a monopod to collect reflectance measurements from 350-1027 nm in increments of 0.38 nm. Calibration of the spectrometer occurred with a standard reflectance panel. A tablet operating CALMIT Data Acquisition Program 2 (CDAP-2, UNL Nutech Ventures, Lincoln, Nebraska) was used to control and integrate the spectral measurement from the spectrometers. Spectrometer held vertically approximately one-half meter over the middle of the two-row plots. Ten scans of the plot were taken and averaged to give a mean reflectance for the entire plot. Post-processing of the collected data were performed through CDAP-2 to generate reflectance

values for each plot. The ground-based measurements on check plots were collected only for 2016 season to compare and contrast against the aerial imagery results.

Aerial Imagery

An IRIS⁺ multirotor (3D Robotics, Berkley, California, USA) and Ritewing Zephyr 3 (Rightwing Rc LLC, Apache Junction, Arizona, USA) fixed wing with a 47-inch wingspan sUAS were used as aerial platforms to mount spectral sensors and collect aerial imagery. The fixed wing had a designed endurance of 30 minutes flight with a payload of up to 400 g; whereas multirotor was designed for approximately five minutes of flight time with a similar payload. A CIR (modified broadband Sony Alpha 5100 (Sony Corporation, Tokyo, Japan)) converted for Blue/Green/NIR bands (Arrow Consulting LLC, Manhattan, Kansas, USA) sensor was utilized with the fixed-wing platform in 2016 and on multirotor in 2017 to collect aerial imagery.

Mission Planning

Mission planning was accomplished through Mission Planner (ArduPilot) and Pix4D Capture (Pix4D, Lausanne, Switzerland) apps that allow easier control and observation of sUAS flight details. sUAS aerial imagery was collected both for 2016 and 2017 season. As mentioned earlier, 2016 data was used to compare and contrast between aerial imagery and ground-based data to quantify SDS on check plots and 2017 data was used to develop correlation and regression function between PI and SDS score and use developed function to ascertain SDS on the whole field scale. The sUAS flights were conducted on 18 August 2016, 8 September 2017, and 13 September 2017, henceforth referred to as flying dates or FD1, FD2, and FD3 respectively. Flights in 2017 occurred two and seven days after SDS scoring and 14 days before scoring in 2016. The entire field was scored with PI values taken. For FD1, CIR images were collected using fixed-wing sUAS. The fixed wing sUAS was programmed to fly at an altitude of 120 m above ground level (AGL) with a front-to-back and side-to-side overlap of 75% following a single grid pattern. For FD2 and FD3, CIR images were collected using quadcopter programmed to fly at 80 m with front-to-back and side-to-side overlap of 75%. The sUAS multirotor with CIR and fixed wing with CIR sensor were programmed to fly at 5 m/s and 18 m/s respectively. Ground control points were set for each field day with GPS locations recorded. Ground control points were used for the correction and optimization of the orthomosaic. Altitudes were selected to optimize spatial resolution and sUAS flight capabilities. The side-to-side and front-to-back overlap were selected based on parameters of generation of an accurate orthomosaic. The weather parameters were atmospherically stable and suitable for flying on each of the three flight days (FD).

Pigment Index

Photosynthesis uses chlorophyll a and b to absorb photon energy for conversion to sugar and fatty acids. Secondary products of the conversion process are reactive oxygen species that can be harmful to plants in high concentrations. Reactive oxygen species are produced in minute amounts in healthy plants because of aerobic metabolism. Stress causes the amount of reactive oxygen species to increase (Hodecker et al., 2018; Kang et al., 2017). Additionally, microorganisms like fungi and bacteria invade the plant tissue by producing a high concentration of reactive oxygen species, which overwhelm the plant's cells defenses to oxidative damage. Reduction of reactive oxygen species occurs through the production of carotenoids, an antioxidant (Kim et al., 2012). The more stressed the plant becomes the more carotenoids produced. Carotenoids absorb and reflect photons in a manner that can be used to assess changes in carotenoid concentrations and therefore has the potential to be used to assess plant stress. Understanding how different pigments (i.e. chlorophyll a and b and carotenoids) absorb and reflect photons within plant material can lead to the development of methods to detect changes in chlorophyll: carotenoid ratios, and potentially assessment of plant stress.

Chlorophyll a and b absorb photons in blue and red regions while carotenoids absorb photons across blue and green regions of the visible light spectrum (Chappelle et al., 1992), represented in Figure 6 (Heliospectra, 2014). Plants also reflect photons very strongly in the NIR region. Measuring

the absorption and reflectance of photons for the assessment of plant health is often done by generating a normalized difference vegetation index (NDVI). NDVI (Equation 3) has been used in the assessment of plant biomass and growth vigor (Granados-Ramírez et al., 2004; Tucker et al., 1985). NDVI however, is not a reliable indicator of plant stress because plant stress and biomass are confounded.

$$NDVI = \frac{R_{NIR} - R_{Red}}{R_{NIR} + R_{Red}} \quad \text{Equation 3}$$

Where:

R_{NIR} = Reflectance in NIR (700 to 1200 nm)

R_{Red} = Reflectance in Red (600 to 700 nm)

Variations of the NDVI have been developed to assess different regions of the visible spectrum and their relationships to plant characteristics. Blue normalized difference vegetation index (BNDVI) and green normalized difference vegetation index (GNDVI) assess the photons reflected in the blue and green regions, respectively. The BNDVI, Equation 5, is primarily determined by chlorophyll concentration, with some influence from the carotenoid content. The GNDVI, Equation 4, is influenced more heavily by the carotenoid concentration and has been used successfully as an indicator of plant health (Gitelson et al., 1996). Individually, either type of NDVI does not accurately or completely assess plant stress because of the confounding influence of biomass on the NDVI value. A new index called Pigment Index (PI), which reduces the confounding influence of biomass, was derived by subtracting the GNDVI from the BNDVI (KSURF Invention Disclosure No. 2016-010, 2016). PI assesses reflectance from blue, green, and NIR regions captured with a modified broadband camera to assess plant stress (Equation 6). PI changes with the changing ratios of carotenoids to chlorophylls. Increased ratios of carotenoids to chlorophylls indicate stress conditions in the plant, or other physiological conditions that lead to changes in chlorophyll: carotenoid ratios, such as the normal progression through growth stages. Low PI values can be a sign of high concentrations of carotenoids, resulting from plant stress.

It was hypothesized that the introduction of stress and reduction of photosynthetic potential in plants suffering from SDS will result in lowered PI-values. To test this hypothesis, an experimental field of soybean with varied levels of SDS was assessed to determine the degree of correlation between SDS and PI values. As symptoms of SDS progress, the plant is unable to photosynthesize at the same rate as healthy plants. The reduction of photosynthesis causes an increase in the blue light reflected. PI reduction due to stress and reduced photosynthetic activity are apparent in early and late stages of disease progression.

$$GNDVI = \frac{R_{NIR} - R_{Green}}{R_{NIR} + R_{Green}} \quad \text{Equation 4}$$

$$BNDVI = \frac{R_{NIR} - R_{Blue}}{R_{NIR} + R_{Blue}} \quad \text{Equation 5}$$

Where

R_{NIR} = Reflectance in NIR (700-1200nm)

R_{Blue} = Reflectance in blue (400-500 nm)

R_{Green} = Reflectance in green (500-600 nm)

$$PI = BNDVI - GNDVI \quad \text{Equation 6}$$

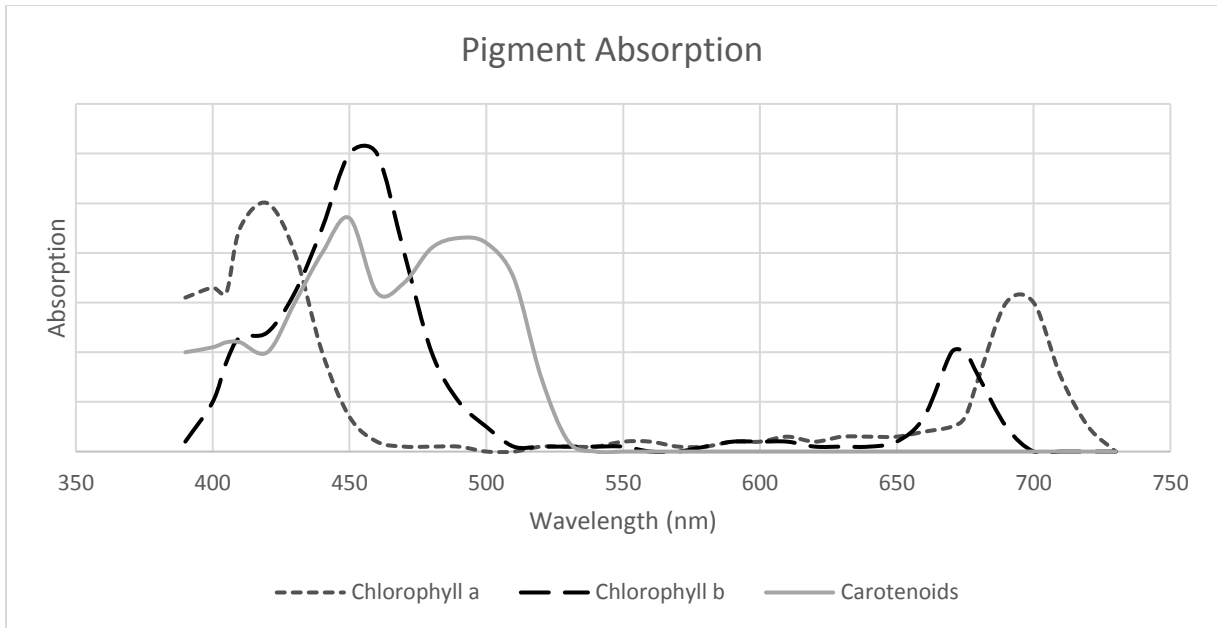


Figure 6 - Absorption bands of Chlorophyll a and b, and carotenoids.

Ground-based Data

Initial processing of the raw spectral data were completed using CDAP-2 software to provide an average reflectance value at each of the collected wavebands for each plot. The ultraviolet wavelength readings were removed from the data. The remaining data were averaged over ten-nanometer bands to reduce the dimensionality of the data set (Phatak, 2004). Blue reflectance was calculated as an average of 465 nm and 475 nm wavebands, green reflectance was calculated as an average of 565 nm and 575 nm wavebands, and NIR reflectance was calculated as an average of 775 nm and 785 nm. These averages were then used to calculate GNDVI, BNDVI, and PI (Equations 3, 4 and 5). PROC CORR used to help select waveband from ground-based data to form indices. Missing scans and bad scans were removed from the dataset; data were then combined with the collected agronomic data, such as SDS score and maturity. Proc Mixed in SAS 9.4 was used to determine if the individual day had significant interaction between the genotype and wavelength. The closest collected day was used which was 8 August 2016 which showed a significant difference between entries and reflectance values.

Aerial Image Processing

Agisoft Photoscan Professional (V 1.2.6, Agisoft LLC, St. Petersburg, Russia) generated an orthomosaic using weighted average values of all pixel reflectance values from individual photos. Ground reference panels were used for geometric correction and accuracy of the orthomosaic. The orthomosaic was then processed in ArcGIS 10.3 (ArcMap 10.4.1, Esri, Redlands, California, USA) to calculate GNDVI, BNDVI, and PI (Equations 3, 4 and 5). Spatial analysis calculated and converted the orthomosaic into GNDVI, BDNVI, and PI maps of the field. The maps were generated with a color gradient of green to red indicating high to low vegetative index values, Figure 7. Transects were established through the approximate center of each row to extract and determine average GNDVI, BNDVI and PI for each plot. The plot scale average vegetative index values observed from aerial and ground-based spectral reflectance data was correlated to SDS scores to ascertain robustness of each method to estimate SDS identification in soybeans (Figure 7)

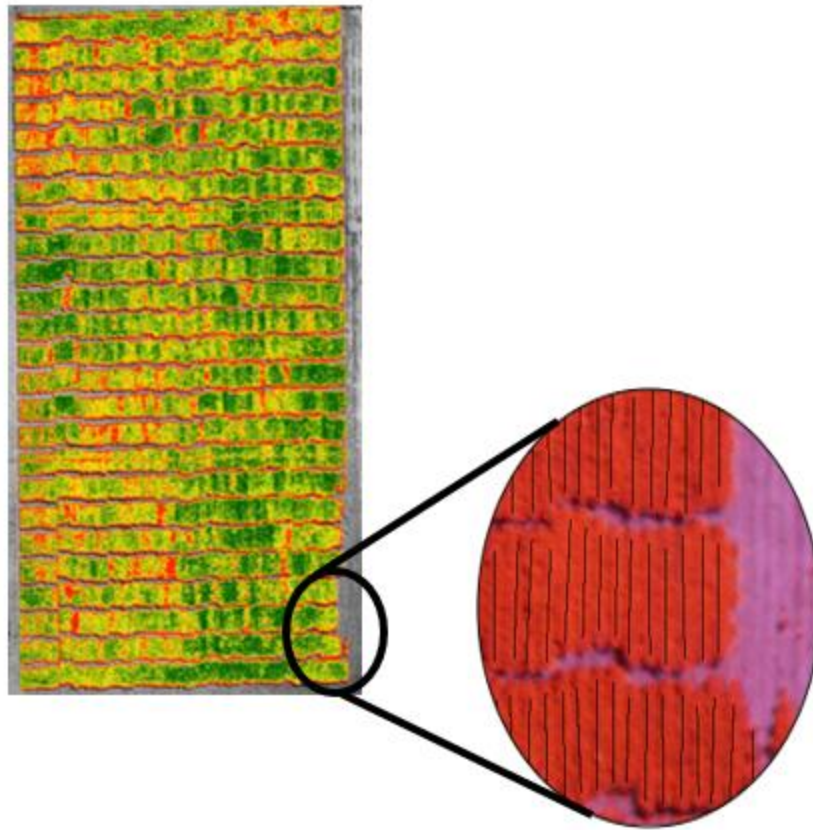


Figure 7 - Example pigment index (PI) map generated using aerial imagery collected on FD1. Green indicates high PI while red indicates low PI. A small sub-section (PI layer turned off for accessibility in transect) shows transects drawn (vertical black lines) across each row.

Results/Discussion

Aerial and ground-based data comparison

Strong correlation between PI and SDS scores was observed within the 2016 check plots with aerial imagery exhibiting slightly stronger correlation ($R^2 = 0.7974$) with SDS scores as compared to ground-based spectrometer data ($R^2 = 0.7809$) (Table 3), however, both showed statistical significance with $P > 0.0001$. Additionally, analysis of only high SDS (SDS scores of ≥ 25) instances using PI indicated significantly higher correlation ($R^2 = 0.8359$) when utilizing aerial imagery (Figure 8) as compared to one from the ground-based data ($R^2 = 0.7114$). sUAS data showed a negative correlation between PI and SDS score while ground-based data show a positive correlation. High SDS scores should show low PI values based on the definition of PI. The positive relationship between ground-based PI and SDS score is believed to be caused by the ground-based system. Aerial data show large changes in the NIR reflectance depending on the plant health while ground-based data does not show the same change in NIR reflectance. This means that PI greatly was influenced by the blue and green reflectance causing a positive relationship with SDS score. Similar behavior was observed in reflectance from ground-based system during multiple studies conducted over the past few years.

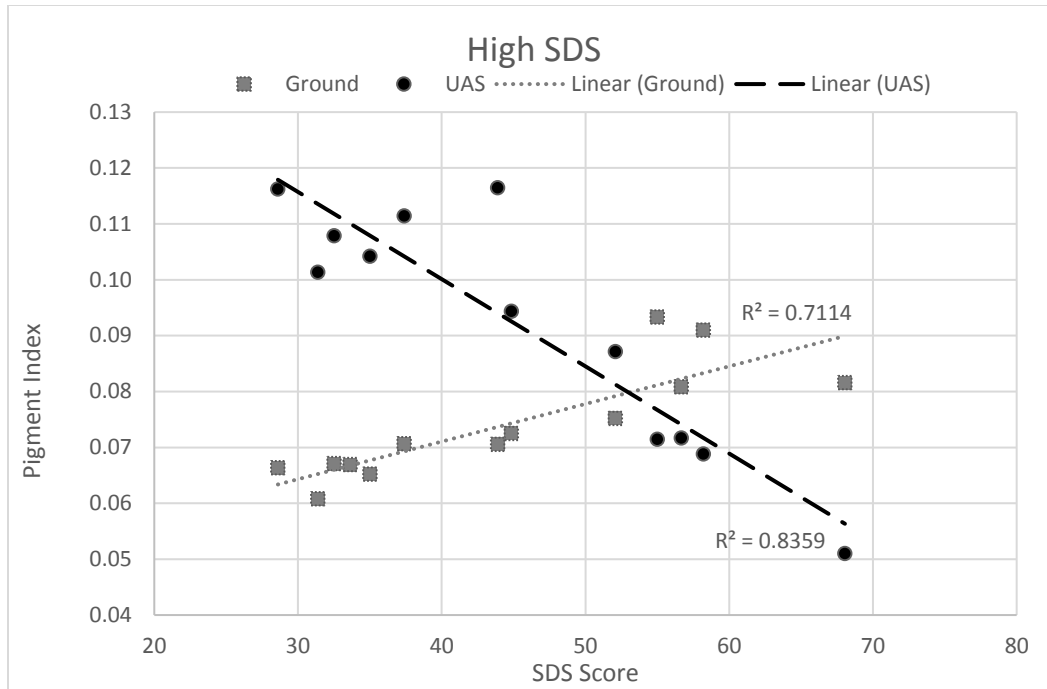


Figure 8 - High SDS score comparison to ground-based and aerial derived PI

The analysis of 2016 check plot with high SDS scores indicated that aerial platforms can be used to conduct spectral analysis to identify SDS susceptible lines more accurately ($R^2 = 0.8359$) than the ground-based unit ($R^2 = 0.7114$). The greater accuracy of aerial system to identify high instances of SDS lines also supported the exclusion of the ground-based unit for the 2017 season and conduct field scale SDS estimation using only aerial imagery. Aerial system can provide breeders, farmers and service providers a means to rapidly assess SDS on spatial scale and implement strategies like selecting desirable genotypes for further breeding, and irrigation management strategies.

Additionally, sUAS missions took considerably less time to collect (average flight time of approximately 11 minutes) aerial imagery than ground-based systems (average four hours) for the same area comprising soybean plots. During short duration of aerial flights, there were minimal change in the temperature, solar angle, wind, and cloud cover as compared to several hours of ground-based system. Therefore, greater accuracy of aerial imagery could be because of the relatively short time frame required to collect aerial imagery and potentially reduced deviations in environmental factors that could influence data quality.

Table 3 – Aerial and ground-based data comparison. R^2 given for SDS score, severity, and incidence given.

Variable	Aerial	Ground-Based
PI	0.7974	0.7809
Severity	0.7547	0.7864
Incidence	0.7451	0.6861

In soybean breeding programs, time available for phenotypic evaluation is one of the largest restraints in breeding new lines. The ability to use sUAS to collect data over a larger area in a short amount of time presents opportunities to analyze a greater number of breeding lines that can be evaluated in a given year. PI derived from check lines plots using ground-based ($R^2 = 0.7809$) and aerial system ($R^2 = 0.7974$) showed high correlation. The regression functions developed using check plots can then be used to predict the performance of the experimental lines

susceptible to SDS on a spatial scale. The estimated SDS values can then be used as the basis of selection. Elimination of lines could be completed with selection based on estimated lower SDS score than that of the susceptible parent (IA3023). This method could allow an increase in the number of lines being evaluated by reducing the number of lines that would need to be physically rated for disease by the breeder, to adjust the parental lines and the SDS checks. The use of aerial imagery and PI could potentially be most useful in early generation screening of large amounts of breeding materials, and subsequent evaluation of selected material by the breeders for resistance before release to ensure the true resistance of the material to SDS.

Comparison of Vegetative Indices to estimates SDS

PI exhibited the highest correlation between three indices GNDVI, BNDVI, and PI when compared to SDS score for FD2 and FD3. GNDVI did not prove to be statistically significant for either FD2 or FD3 (Table 4). GDNVI was not differentiable among high and low SDS scores. Also, SDS infected plants showed the same GNDVI value as healthy plants. BNDVI showed statistical significance for both days; however, the correlation values (-0.3627 and -0.3500 for FD2 and FD3) were considerably lower than the PI (-0.7916 and -0.7163 for FD2 and FD3 Table 4). The results highlighted that PI could be a more robust vegetative index than NDVI to correlate SDS disease identification in soybean at spatial scale.

Table 4 - Spearman's Rho of GNDVI, BNDVI, and PI for FD2 and FD3. Statistically significant values (P < 0.001) are noted given an asterisk

DAY	GNDVI	BNDVI	PI
FD2	-0.0838	-0.3627*	-0.7916*
FD3	-0.0743	-0.3500*	-0.7163*

Breeding programs will eliminate the genotypes with the highest response to SDS and develop others to further increase resistance to SDS for the next season. In 2016, only 16 of the 160 plots scored high for SDS infection, as a result, the 2017 data was used to assess the ability of PI to identify plots with high SDS for elimination. From 2017 data, the top 50% of the plots with the highest SDS scores were selected and compared with plots with bottom 50% of PI values to quantify percentage of SDS plots identified correctly using the PI. PI as an indicator should identify the same plots as highly infected as the SDS score identifies. SDS scores for selected plots ranged from 93.83 to 29.60. PI from FD2 recognized 80.0% of top 50% SDS infected plots in the analysis. FD3's PI values accounted for 78.75% of the plots. BNDVI correctly identified 68.75% and 72.5% of the top plots for FD2 and FD3 respectively. GNDVI only identified 53.75% and 63.75% correctly for FD2 and FD3 respectively. The decrease in correlation from FD2 to FD3 can be accounted for based on the senescence of the plants. R6 occurs very close to maturity of the soybeans. Within 10 days of R6, plants are reaching maturity and as a result, photosynthesis in the plant is slowing. The PI does not differentiate between low PI caused by high SDS infection and senescence of the plant. PI is a good indicator of SDS however, results indicated that it is important to use it at the proper growth stage. The comparison of results from the two FD in 2017 showed that PI could provide stronger correlation to SDS if the aerial imagery is collected when SDS leaf systems are fully visible and before plant senescence. Overall, the results indicated PI is a robust vegetative index which can assist both breeders and farmers in identifying high SDS infected soybeans with high confidence on a spatial scale.

Incidence and Severity Estimates

For aerial assessment of SDS to be practically applied, the whole field must display a correlation of PI to SDS score. The whole field analysis to quantify SDS using SDS scores in 2017 was statistically significant (P > 0.0001) and indicated strong correlation for both FD2 (ρ = -0.7916) for FD3 (ρ = -0.7163) as shown in Figure 9.

SDS score was further analyzed by breaking SDS score into its components, severity and incidence and correlation to PI were determined. Severity presented greater correlation, than incidence and SDS score (Figure 10). FD2 and FD3 displayed lower variance and higher correlations with $R^2 = 0.6313$ and $\rho = -0.8016$ and $R^2 = 0.5153$ and $\rho = -0.7389$, respectively. Both variance and correlation between severity and PI are improved from the variance and correlation of SDS score and PI for both FD2 and FD3. Incidence presented a lower correlation ($\rho = -0.7185$ for FD2 and $\rho = -0.6774$ for FD3) and higher variance for both days (Figure 11) compared to severity.

Large-scale operations will not take into consideration the incidence of infection because small plots are not planted on large farming operations. Farming operations will not determine the amount of SDS present, only that SDS is present. Once SDS presence is determined in a field mitigation steps will be taken to decrease the impact of SDS on yield over the whole field rather than a small portion. While SDS score and incidence are great disease indicators for small research plots, while severity is applicable no matter the size of the field. And provide greater application opportunities.

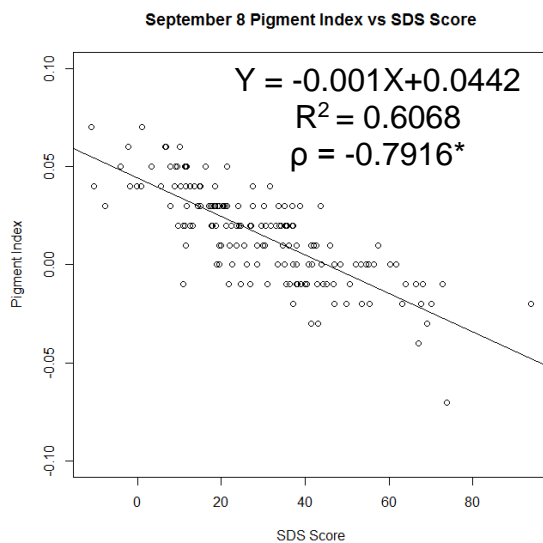


Figure 9 – 8 September 2017 PI comparison with SDS score. The equation for line of fit, R^2 , and Spearman's rho (ρ) are given. Correlation coefficients that statistically significant ($P < 0.0001$) are indicated by an asterisk.

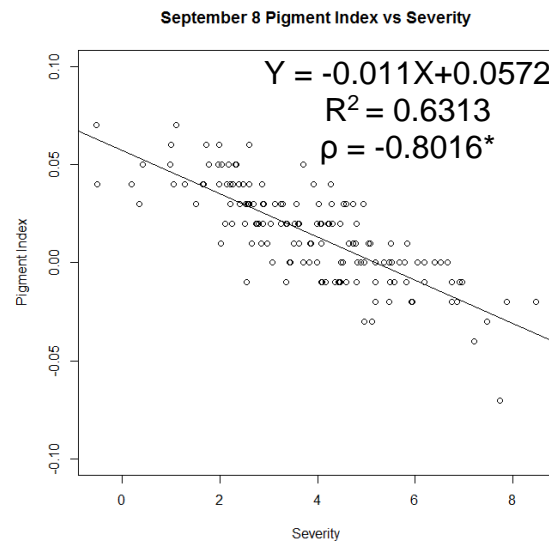


Figure 10 – 8 September 2017 severity as compared to PI. The equation for line of fit, R^2 , and Spearman's rho (ρ) are given. Correlation coefficients that statistically significant ($P < 0.0001$) are indicated by an asterisk.

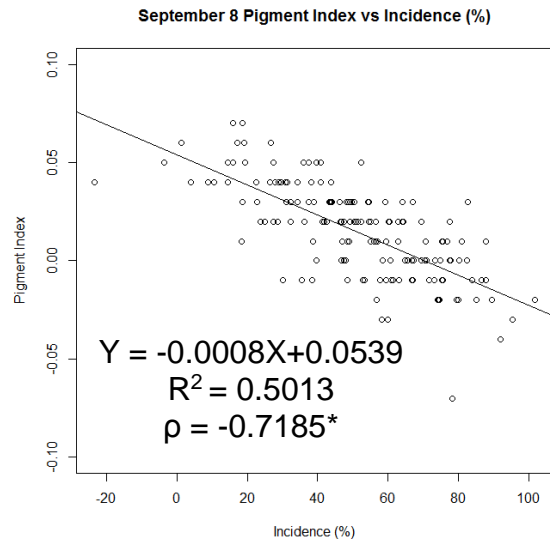


Figure 11 – 8 September 2017 incidence as compared to PI. The equation for line of fit, R^2 , and Spearman’s rho (ρ) are given. Correlation coefficients that statistically significant ($P < 0.0001$) are indicated by an asterisk.

Area coverage

The strong correlation between PI and SDS scores indicated that the aerial imagery could be used to derive PI for quantification of SDS on soybean. The comparable results from aerial imagery and ground-based data also indicated that sUAS aerial imagery based PI can provide comparable results to quantify SDS. The sUAS aerial imaging system can potentially cover much larger area compared to the ground-based system within a time duration available in a day. The aerial systems presented in this study are capable of covering approximately 6 hectares per hour while only 0.33 hectare per hour could be covered with the ground-based system. The reduction in time spent on SDS assessment translates to increased productivity and opportunity to cover larger plots multiple times in a growing season. Overall, sUAS system can provide an opportunity to breeders for conducting high spatial and temporal studies covering greater number of breeding lines during the growing season.

Conclusion

Previous studies showed that thermal assessment of disease was possible through aerial platforms. The case study presented here demonstrates that an infield assessment and accurate identification of soybean SDS using a TIR camera and sUAS system is possible. Correlations with temperature difference and SDS score increased along with severity throughout the growing season. Correlations with disease incidence and severity also presented increases through the growing season with very strong correlations at the end of the season. Overall assessment of incidence displayed the highest relationship in correlation over the days flown while severity maintained a similar relationship. Severity of SDS infection is the most practical predictor of SDS for large application use because of its high correlation and easy application.

This case study exhibits the potential use of TIR remote sensing for detection of SDS in soybean. While correlations at the beginning of the flight period were moderate, they have potential to act as predictors to SDS within a field and give preliminary indications of the disease before visual symptoms appear. Future studies will expand this research to assess disease over an entire field and determine when the earliest that definable SDS symptoms are present.

This study also exhibited that aerial SDS assessment using a sUAS data collection method is statistically comparable to ground-based data collection methods, and SDS is quantifiable from aerial

platforms over a whole field. PI acts as an indicator of SDS indirectly correlating to SDS presence. Aerial imagery derived PI derived using aerial imagery showed a strong negative correlation to the SDS scores for checks and high scoring SDS plots in 2016. Analysis of PI from aerial imagery as a detector of SDS provided results comparable to ground-based system. Decreased variability in the ground-based scores was explained with the selection of individual wavelengths in the calculation of ground-based BNDVI, GNDVI, and PI. Overall, the aerial imaging systems can provide field data in a relatively short amount of time with potentially minimal environmental variability and improved SDS estimation through PI as compared to the ground-based collected data.

Aerial PI also presented a strong correlation over a whole field in the 2017 growing season. Individual components of SDS score, severity, and incidence were analyzed to assess their strength as measurements of SDS. SDS severity maintained the least variability and highest correlation to PI across the 2017 data including SDS score. PI detection of severity is a promising indicator of SDS and applicable across all field sizes including large farming operations. Future studies will include an early assessment of SDS to determine if SDS is detectable through CIR imagery before visible symptoms appear.